DOI: 10.1002/chem.200902997

Photomagnetic Switching of Heterometallic Complexes $[M(dmf)_4(H_2O)_3(\mu\text{-}CN)Fe(CN)_5]\cdot H_2O$ (M = Nd, La, Gd, Y) Analyzed by Single-Crystal X-ray Diffraction and Ab Initio Theory

Helle Svendsen,[a] Jacob Overgaard,[a] Marie A. Chevallier,[a] Eric Collet,[b] Yu-Sheng Chen,[c] Frank Jensen,[a] and Bo B. Iversen*[a]

Abstract: Single-crystal X-ray diffraction measurements have been carried out on $[Nd(dmf)_4(H_2O)_3(\mu\text{-}CN)Fe(CN)_5]\cdot H_2O$ (**1**; dmf = dimethylformamide), $[Nd(dmf)_4(H_2O)_3(\mu\text{-}CN)Co(CN)_5]\cdot H_2O$ (**2**), $[La(dmf)_4(H_2O)_3(\mu\text{-}CN)Fe(CN)_5]\cdot H_2O$ (**3**), $[Gd(dmf)_4(H_2O)_3(\mu\text{-}CN)Fe(CN)_5]\cdot H_2O$ (**4**), and $[Y(dmf)_4(H_2O)_3(\mu\text{-}CN)Fe(CN)_5]\cdot H_2O$ (**5**), at 15(2) K with and without UV illumination of the crystals. Significant changes in unit-cell parameters were observed for all the iron-containing complexes, whereas **2** showed no response to UV illumination. Photoexcited crystal structures have been determined for **1**, **3**, and **4** based on refinements of two-conformer models, and excited-state occupancies of 78.6(1), 84(6), and 86.6(7) % were reached, respectively. Significant bond-length changes were observed for the Fe–ligand bonds (up to 0.19 Å), the cyano bonds (up to 0.09 Å), and the lanthanide–ligand bonds (up to 0.10 Å). Ab initio theoretical calculations were carried out for the experimental ground-state geometry of **1** to understand the electronic structure changes upon UV illumination. The calculations suggest that UV illumination gives a charge transfer from the cyano groups on the iron atom to the lanthanide ion moiety, $\{Nd(dmf)_4(H_2O)_3\}$, with a distance of approximately 6 Å from the iron atom. The charge transfer is accompanied by a reorganization of the spin state on the $\{Fe(CN)_6\}$ complex, and a change in geometry that produces a metastable charge-transfer state with an increased number of unpaired electrons, thus accounting for the observed photomagnetic effect.

Keywords: charge transfer · heterometallic complexes · magnetic properties · structure elucidation · X-ray diffraction

Introduction

Development of new materials with tailored physical properties controlled by external stimuli has recently been given increased attention. Light irradiation represents one of the main external perturbations and many different types of photoswitchable molecular systems have been investigated. The excited states can be stabilized from microseconds to days due to structural degrees of freedom that are coupled to an electronic excitation. A unique experimental access to such excited-state structural changes is provided by photocrystallography, which is a rapidly evolving branch of modern crystallography.[1] The lifetime of the excited state dictates how challenging the experiments are. Short lifetimes (< ms) require the use of time-resolved diffraction, whereas long-lived states can be studied by normal diffraction experiments (steady-state method).[2] Several ligand isomerization effects have been studied by steady-state methods.[3–6] Spin-transition compounds have also been studied extensively, through which structural changes have been observed in Fe-containing complexes with light-induced excited spin-state trapping (LIESST) properties.[1b,d–e,7,8] Observation of the electron redistribution in such a photoinduced excited high-spin (HS) state has also recently been reported.[9] A further study of such spin-crossover systems revealed a se-

[a] H. Svendsen, Dr. J. Overgaard, M. A. Chevallier, Prof. Dr. F. Jensen, Prof. Dr. B. B. Iversen
Centre for Materials Crystallography
Department of Chemistry and iNANO
University of Aarhus, 8000 Århus C (Denmark)
Fax: (+45) 8619-6199
E-mail: bo@chem.au.dk

[b] Prof. Dr. E. Collet
Institut de Physique de Rennes, Université de Rennes1
UMR UR1-CNRS 6251, 35000 Rennes (France)

[c] Dr. Y.-S. Chen
ChemMatCARS Beam Line, The University of Chicago
Advanced Photon Source, Argonne, IL 60439 (USA)

lective switch between three different states (LS–LS, HS–LS, HS–HS) in a dinuclear spin-crossover compound by tuning the laser excitation wavelength.[10] At the other end of the timescale, microsecond time-resolved diffraction experiments have been carried out[11] and structural reorganizations were observed even with picosecond resolution.[12]

Photomagnetic materials are a class of compounds that show changes in their magnetic properties upon light stimulation. Various photomagnetic phenomena have been observed, such as photoinduced magnetization, demagnetization, spin flipping, and so forth,[13] and these are interesting properties in relation to developing new memory devices.[14] Earlier, much focus was on Prussian Blue analogues,[15] but other types of complexes are currently being investigated.[16] In 2003, Li et al. studied a cyanide-bridged heterobimetallic complex containing neodymium and iron, $[Nd(dmf)_4(H_2O)_3(\mu\text{-}CN)Fe(CN)_5]\cdot H_2O$ (**1**; dmf = *N*,*N*-dimethylformamide; Scheme 1), which exhibits a large increase of the magnetic

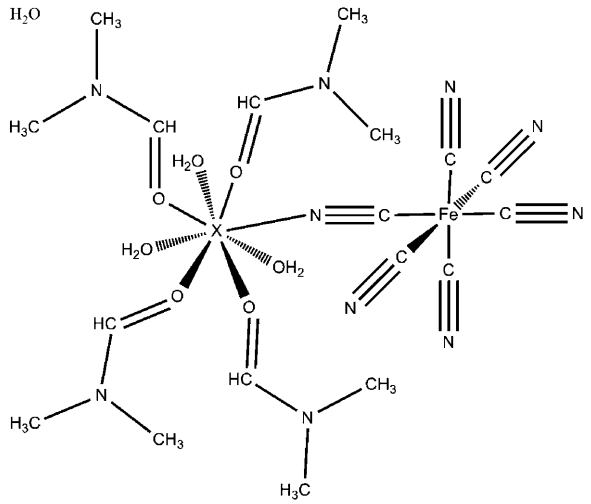

Scheme 1. The molecular asymmetrical unit of $[X(dmf)_4(H_2O)_3(\mu\text{-}CN)Fe(CN)_5]\cdot H_2O$ with X being a yttrium or lanthanide atom.

susceptibility upon illumination with UV light at low temperatures ($T < \approx 50$ K).[17] A number of isostructural complexes with metal substitution as well as related 3d–4f complexes have since been synthesized,[18] but their photomagnetic behavior upon light illumination has not been probed. Photoinduced changes in the magnetization has been confirmed in only two other related complexes, $[Nd(dmf)_4(H_2O)_3(\mu\text{-}CN)Co(CN)_5]\cdot H_2O$ (**2**)[19] and $[Nd(hp)_4(H_2O)_3(\mu\text{-}CN)Fe(CN)_5]\cdot H_2O$ (hp = 4-hydroxypyridine),[20] both showing an enhancement in the magnetic susceptibility upon visible-light and UV-light illumination, respectively.

The nature of the electronic transition, which causes the change in the magnetic properties in **1** is not known. The excited state of **1** is metastable with a lifetime of several hours at temperatures below 50 K,[17] and this made it possible for us to measure the ground- and excited-state crystal structures using conventional very-low-temperature crystallographic techniques.[21] The observed structural changes indicated which part of the molecule is involved in the electronic transition, and the largest modifications were found around the iron atom, where all the iron–ligand bond lengths decreased (Fe–C), whereas a corresponding C≡N bond length increase was observed in the cyano ligands. This indicated that the iron atom must play an important role in the excitation process.

Since the susceptibility increases upon UV illumination, a process that increases the magnetic moment must take place. This can happen by introducing more unpaired spins on the metal ions, by either 1) a metal-to-metal charge transfer (MMCT), 2) a ligand-to-metal charge transfer (LMCT), 3) a spin crossover from LS to HS, or d) a change in the magnetic coupling between Nd and Fe, which has been found to be antiferromagnetic in **1**.[22] In the latter case the excitation may strengthen the 3d–4f coupling or potentially even change it to a ferromagnetic coupling. Mössbauer spectroscopy data was used to rule out a MMCT mechanism, and they showed a decrease in the quadrupole splitting, which indicated a possible distortion of the $\{Fe^{III}(CN)_6\}$ moiety. UV and IR spectra showed changes in the excited state, which was interpreted by Li et al. as an increase in the electron density on Fe^{III}.[17] Based on these results, Li et al. suggested that a LMCT on the iron ion was the result of the UV illumination and the source of the increase in magnetic susceptibility. Due to the shorter bond lengths around Fe in the excited state observed by the photocrystallographic experiments, a spin crossover explanation was discarded.[21] If a LMCT on Fe occurs, charge is transferred from the ligands to the iron atom, and due to strong back donation from the cyano ligands, the Fe^{2+}–C bond lengths are expected to be shorter than in Fe^{3+}–C in the $Fe(CN)_6$ moiety.[23] The excited-state structure of **1** did clearly show a decrease in the iron–ligand bond lengths. However, if a LMCT on iron is occurring this will not increase the magnetization, since ligand donation into the low spin t_{2g} orbitals occupied by five electrons will decrease the number of unpaired electrons. Similarly, donation into the antibonding e_g orbitals will increase the Fe–C bond length at variance with experiments. LMCT on iron therefore does not seem to be a possible cause of the photomagnetic effect. A change in the intramolecular magnetic coupling could not be ruled out by the observed structural changes, as a significantly shorter distance between the metal centers was observed in the excited state.[21]

To further investigate the photomagnetic effect, we present results from new photocrystallographic studies of four isostructural complexes: $[Nd(dmf)_4(H_2O)_3(\mu\text{-}CN)Co(CN)_5]\cdot H_2O$ (**2**), $[La(dmf)_4(H_2O)_3(\mu\text{-}CN)Fe(CN)_5]\cdot H_2O$ (**3**), $[Gd(dmf)_4(H_2O)_3(\mu\text{-}CN)Fe(CN)_5]\cdot H_2O$ (**4**), and $[Y(dmf)_4(H_2O)_3(\mu\text{-}CN)Fe(CN)_5]\cdot H_2O$ (**5**). For each system, complete single-crystal X-ray data sets were collected every three hours on the crystals kept at 15 K. The first data set was measured without UV light, whereas the remaining sets of data were collected with continuous illumination. The results are compared to our earlier results obtained for **1**.[21] We also report ab initio theoretical analysis of the excitation of **1** using the experimentally determined ground-state structure.

Table 1. Crystallographic data and refinement residuals for **3**, **4**, and **5**.

	Complex **3**		Complex **4**		Complex **5**	
collected data	0	4	0	5	0	3
space group	$P2_1/n$	$P2_1/n$	$P2_1/n$	$P2_1/n$	$P2_1/c$	$P2_1/c$
T [K]	10(2)	10(2)	10(2)	10(2)	10(2)	10(2)
a [Å]	17.7235(9)	17.452(1)	17.6036(5)	17.3791(8)	13.884(1)	13.773(2)
b [Å]	8.8652(4)	8.8078(5)	8.7949(3)	8.7614(3)	8.84(1)	8.769(1)
c [Å]	19.459(9)	19.485(1)	19.3934(5)	19.4633(7)	24.601(2)	24.305(4)
β [°]	96.193(2)	97.088(5)	96.384(2)	96.966(3)	96.750(6)	95.866(8)
V [Å^3]	3039.6(2)	2972.2(3)	2983.9(2)	2941.7(2)	2998.5(2)	2920.1(11)
λ [Å]	0.71073	0.71073	0.71073	0.71073	0.71073	0.71073
Z	4	4	4	4	4	4
μ [mm^{-1}]	1.959	1.959	2.75	2.75	2.465	2.465
N_{ref}	23240	27573	27957	27297	27084	26281
N_{unique}	9743	9584	9632	9435	9586	9767
R_{int}	0.0906	0.1398	0.0367	0.0678	0.0973	0.5524
N_{params}	333	164	343	294	343	–
N_{obsd} (2σ)	4055	1989	6519	3066	3785	–
R_{all}	0.1144	0.2663	0.051	0.1459	0.1245	–
$R(F)$ (2σ)	0.0398	0.0601	0.0272	0.0472	0.0359	–
$R_w(F^2)$ (2σ)	0.068	0.1233	0.0582	0.1131	0.0638	–
GOF	0.605	0.908	0.692	0.841	0.514	–

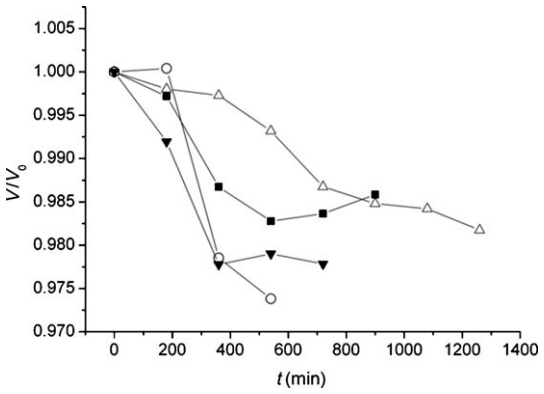

Figure 1. Unit-cell volume of **1** (△), **3** (▼), **4** (■), and **5** (○) as a function of time. The laser is turned on at $t=0$ min. The estimated standard deviations are smaller than the symbols used in the plot.

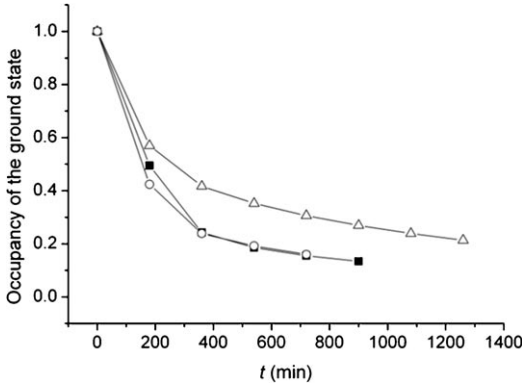

Figure 2. The occupancy of the ground state of **1** (△), **3** (○), and **4** (■) as a function of time. The laser is turned on only after the first data point has been measured.

Results and Discussion

Photocrystallographic results: Table 1 lists selected details from the crystallographic refinements. In the following discussion the results from our earlier photocrystallographic measurements of **1** are included for comparison.[21] In Figure 1 normalized unit-cell volumes of **1**, **3**, **4**, and **5** are plotted as a function of time. Compound **2** did not show any changes in the unit-cell parameters as a function of time when illuminated with UV light and is therefore not included in the figure. This is consistent with the fact that **2** should only be photomagnetic upon visible-light illumination, hence no changes are expected to occur upon UV illumination. Instead significant changes in the unit-cell volume are observed for all the Fe-containing complexes with a largest decrease of approximately 2.5% in the volume of **5** after approximately 9 h. This strongly indicates that these systems have been successfully photoexcited. Since the excited-state occupancies (Figure 2) and unit-cell dimensions are still slowly changing in the last data collection for all complexes, complete excitation of the crystals has not been achieved.

Figure 2 shows the occupancy of the ground state of **1**, **3**, and **4** as a function of time. The occupancy for each complex arises from the refinement of a model containing two molecular conformers. Unfortunately, it was not possible to obtain a reasonable two-conformer model for **5** in the excited state due to poor data quality, and hence this complex is omitted in the remaining discussion. Figure 1 reveals that the yttrium-containing complex behaves differently from the lanthanide complexes, although it still has a clear response to the UV-light illumination as shown by the unit-cell contraction. Complex **4** shows the largest photoconversion with a ground-state occupancy of 13.4% in the last data collection. As observed for the cell changes, saturation in the occupancy is not completely reached for any of the complexes. The photoconversion may therefore not exceed approximately 85% with the current setup, which differs significantly from the original setup by Li et al. who used a powder sample in-

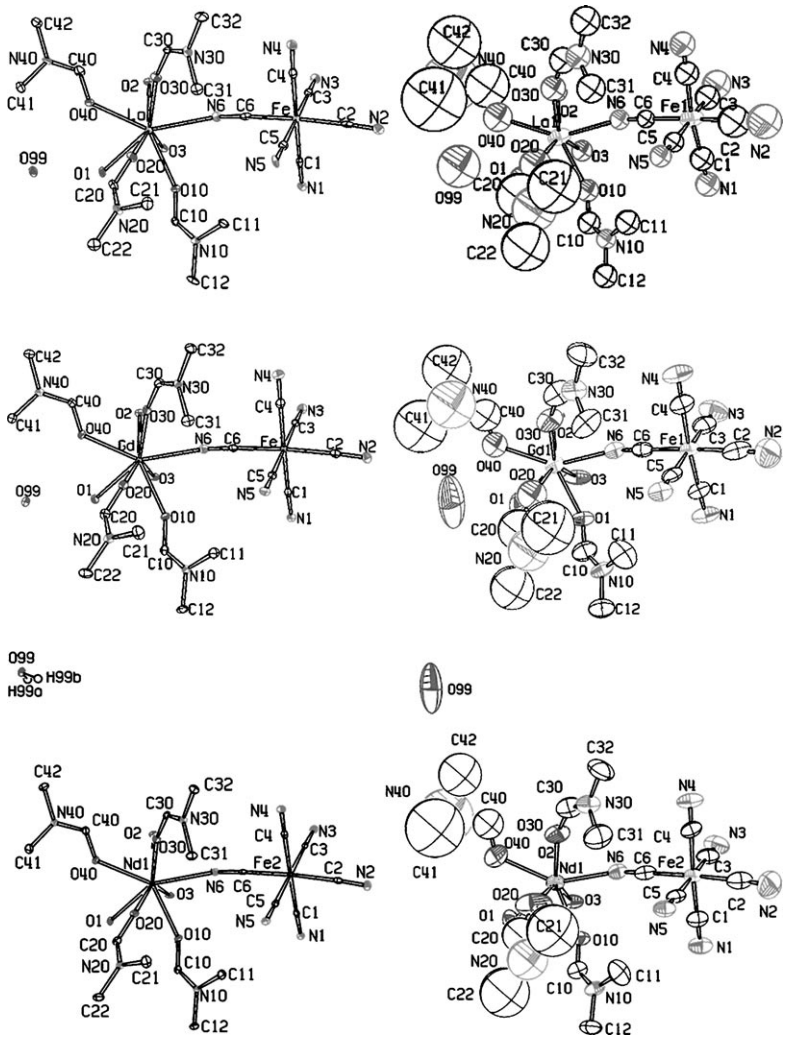

Figure 3. The ground-state (left) and excited-state (right) structures of **1** (bottom), **3** (top), and **4** (middle) with atomic displacement ellipsoids drawn at the 50% probability level. H atoms are omitted for clarity. For **1** the structures are taken from ref. [21], and they are included for comparison.

stead of a single crystal as used in the present photocrystallographic experiments.[12]

Figure 3 shows thermal ellipsoid drawings (ORTEPs) of the ground-state and excited-state structures of **1**, **3**, and **4**, and the structural data reveal significant bond-length changes upon excitation. The metal–ligand bond lengths as well as the cyano bond lengths for the three complexes are listed in Table 2 for both the ground-state and excited-state structures. The structural changes of **3** and **4** are very similar to the changes observed in **1**. The largest changes are found around the Fe atom in **3** with a maximal decrease of 9.2% (corresponding to 0.19 Å) for the Fe–C2 bond and an increase of 4.4% (0.06 Å) in the C3–N3 cyano bond. For each of the complexes the trends in the bond-length changes are very similar: The largest changes are found around the Fe atoms, especially the Fe–C2 and Fe–C3 bonds, and a decrease in an Fe–C bond is always accompanied by a similar increase in the corresponding C≡N cyano bond length. This is illustrated in Figure 4, in which the percentage changes in bond lengths for Fe–C and C≡N for each of the complexes are given. The graph is quite symmetric around 0% bond-length change, which indicates the relation between a decrease in the Fe–C bond length and a corresponding increase in the C≡N bond length.

The changes around the lanthanide atoms are not as large as around the iron atom, but a highly significant decrease is observed for the bridging X–N6 bond in all of the complexes. Some of the lanthanide–dmf ligand bond lengths increase, especially the X–O40, and to a lesser extent the X–O20. Several bond lengths also increase within these two dmf molecules, which are located far from the metal centers. The dmf molecules are completely ordered in the ground-state structure, but in the excited-state structures of **1**, **3**, and **4** the atoms in the two dmf groups show unusually large thermal ellipsoids as shown in Figure 3. Large ellipsoids may be a sign of structural disorder, but we have not been able to refine a dmf model with two conformations in the excited state in any of the structures. Overall, there is a large, but fairly uniform increase in the atomic displacement parame-

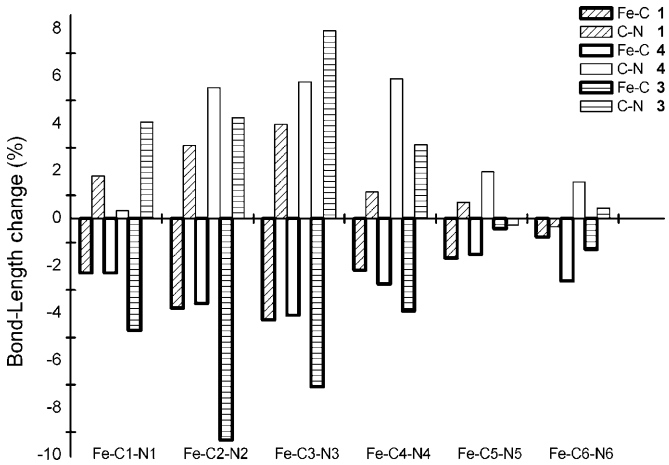

Figure 4. Bond-length changes in the cyanide groups in **1**, **3**, and **4**.

Table 2. Metal–ligand bond lengths and cyano bond lengths in the ground state (refinement of the first data collection) and the excited state (refinement of the last data collection) in **3** and **4**, including the ratio and percentage change between the ground- and excited-state bond lengths. The bond lengths of **1** from ref. [21] are included for comparison.

	Complex **3**				Complex **4**			
Bond	Ground state [Å]	Excited state [Å]	Ratio	Change [%]	Ground state [Å]	Excited state [Å]	Ratio	Change [%]
X–N6	2.624(4)	2.542(9)	0.969(4)	−3.1(3)	2.494(3)	2.434(7)	0.976(3)	−2.4(3)
X–O1	2.532(3)	2.531(9)	1.000(4)	0.0(4)	2.399(2)	2.389(5)	0.996(2)	−0.4(2)
X–O2	2.496(2)	2.472(6)	0.990(3)	−1.0(3)	2.394(2)	2.370(5)	0.990(2)	−1.0(2)
X–O3	2.528(2)	2.496(7)	0.987(3)	−1.3(3)	2.419(2)	2.396(5)	0.991(2)	−0.9(2)
X–O10	2.469(3)	2.449(7)	0.992(3)	−0.8(3)	2.374(2)	2.372(5)	0.999(2)	−0.1(2)
X–O20	2.493(2)	2.553(10)	1.024(4)	2.4(4)	2.380(2)	2.445(9)	1.027(4)	2.7(4)
X–O30	2.455(3)	2.431(8)	0.990(3)	−1.0(3)	2.352(2)	2.335(6)	0.993(3)	−0.7(3)
X–O40	2.488(3)	2.597(10)	1.044(4)	4.4(5)	2.392(2)	2.479(7)	1.036(3)	3.6(3)
Fe–C1	1.930(4)	1.84(1)	0.954(7)	−4.7(7)	1.930(3)	1.886(8)	0.977(4)	−2.3(4)
Fe–C2	1.939(4)	1.76(2)	0.907(10)	−9.3(10)	1.936(3)	1.867(11)	0.964(6)	−3.6(6)
Fe–C3	1.965(4)	1.83(1)	0.929(7)	−7.1(7)	1.946(3)	1.867(11)	0.959(6)	−4.1(6)
Fe–C4	1.950(4)	1.87(1)	0.961(7)	−3.9(7)	1.933(3)	1.880(9)	0.973(5)	−2.7(5)
Fe–C5	1.940(4)	1.93(1)	0.996(6)	−0.4(6)	1.941(3)	1.912(9)	0.985(5)	−1.5(5)
Fe–C6	1.941(4)	1.92(1)	0.987(6)	−1.3(6)	1.944(2)	1.893(9)	0.974(5)	−2.6(5)
C1–N1	1.148(5)	1.20(1)	1.04(1)	4.1(12)	1.158(3)	1.162(9)	1.003(8)	0.3(8)
C2–N2	1.146(5)	1.20(2)	1.04(2)	4.3(16)	1.156(3)	1.220(12)	1.055(11)	5.5(11)
C3–N3	1.144(5)	1.24(1)	1.08(1)	8.0(13)	1.157(3)	1.224(11)	1.058(9)	5.8(10)
C4–N4	1.152(5)	1.19(1)	1.03(1)	3.1(12)	1.152(3)	1.220(9)	1.059(9)	5.9(8)
C5–N5	1.151(5)	1.15(10)	0.997(10)	−0.3(10)	1.156(3)	1.179(9)	1.020(9)	2.0(8)
C6–N6	1.138(5)	1.143(9)	1.004(10)	0.4(9)	1.154(3)	1.172(9)	1.016(9)	1.6(8)

	Complex **1**			
Bond	Ground state [Å]	Excited state [Å]	Ratio	Change [%]
X–N6	2.557(2)	2.476(6)	0.968(2)	−3.2(2)
X–O1	2.459(1)	2.481(5)	1.009(2)	0.9(2)
X–O2	2.451(1)	2.431(4)	0.992(2)	−0.8(2)
X–O3	2.479(1)	2.479(4)	1.000(2)	0.0(2)
X–O10	2.421(1)	2.384(5)	0.985(2)	−1.5(2)
X–O20	2.432(1)	2.454(6)	1.009(3)	0.9(3)
X–O30	2.401(1)	2.364(5)	0.985(2)	−1.5(2)
X–O40	2.439(1)	2.539(6)	1.041(3)	4.1(3)
Fe–C1	1.935(2)	1.891(8)	0.977(4)	−2.3(4)
Fe–C2	1.939(2)	1.866(10)	0.962(5)	−3.8(5)
Fe–C3	1.946(2)	1.863(9)	0.957(5)	−4.3(5)
Fe–C4	1.939(2)	1.897(7)	0.978(4)	−2.2(4)
Fe–C5	1.943(2)	1.911(8)	0.984(4)	−1.6(4)
Fe–C6	1.945(2)	1.930(8)	0.992(4)	−0.8(4)
C1–N1	1.157(2)	1.178(8)	1.018(7)	1.8(7)
C2–N2	1.159(2)	1.195(10)	1.031(9)	3.1(9)
C3–N3	1.154(2)	1.200(9)	1.040(8)	4.0(8)
C4–N4	1.152(2)	1.165(8)	1.011(7)	1.1(7)
C5–N5	1.152(2)	1.160(8)	1.007(7)	0.7(7)
C6–N6	1.155(2)	1.151(8)	0.997(7)	−0.4(7)

ters (ADPs) on all atoms of the excited-state structures. The origin of this increase is unclear, but it is noteworthy that it is observed for all three different crystal structures, and indeed large increases in the ADPs have also been observed for other reported structures of metastable states.[9,24] A competing effect between an excitation and a heating resulting from the light exposure could be present. However, the relatively large decrease in unit-cell parameters indicates a clear dominance of the excitation effect. The large ADPs may reflect that two (or more) very similar metastable minima are reached upon excitation with slightly differing nuclear configurations. The large ADPs in the excited-state structures could be enhanced by overestimation of the occupancy parameters, since an increase in the excited-state occupancy parameter can be offset by adding additional "thermal smearing". This can have an influence on the accuracy of the occupancy parameter in each data collection for each complex, but the relative changes in the occupancy between each data collection should still be valid. Hence the shapes of the occupancy curves in Figure 2 should remain the same, but they may be shifted to slightly larger values. The main conclusion for the structural changes in the excited state is that the iron–ligand bond lengths decrease while the CN bond lengths increase. Furthermore, molecular disorder appears to be present in the dmf ligands in the excited state. Overall it can be concluded that **1**, **3**, and **4** show very similar structural changes upon UV excitation. In the case of **5** a clear response to UV excitation is observed in the form of very large unit-cell changes, but refinement of the excited-state crystal structure has not yet been possible. It should be

stressed that actual photomagnetization has so far only been measured for **1**.

Theoretical analysis: To obtain insight into the electronic changes responsible for the change in the magnetic moment upon excitation, ab initio electronic structure calculations have been performed on the molecular complex **1**. The isolated Nd complex has a high-spin f^3 electron configuration, while the $\{Fe(CN)_6\}$ complex has a low-spin d^5 electron configuration. An antiferromagnetic coupling (AF) of these configurations results in a net magnetic moment corresponding to $S=1$, while a ferromagnetic coupling (FC) results in a magnetic moment corresponding to $S=2$. These states are denoted $^3\Psi_n$ and $^5\Psi_n$, respectively. An initial exploration at the Hartree–Fock (HF) and density functional (B3LYP) levels suggested that there are low-energy charge-transfer states with the Nd complex having a high-spin f^4 electron configuration and the $\{Fe(CN)_6\}$ complex having an intermediate-spin d^4 electron configuration. Coupling of these configurations leads to two states with $S=1$ and $S=3$, and we have in addition also considered a state with $S=2$ corresponding to the $\{Fe(CN)_6\}$ complex having a net spin of zero. These states are denoted $^3\Psi_{ct}$, $^7\Psi_{ct}$, and $^5\Psi_{ct}$, respectively.

The relative energies of these five states at the experimental ground-state geometry are shown in Table 3 as a function of theoretical level using effective core potentials for Nd, Fe, C, N, and O and a polarized valence double-zeta-type basis set. The energy difference between an AF or FC coupling of the two spin centers is calculated to be only a few kilojoules per mole for both the normal and charge-transfer states (relative energies of $^3\Psi_n/^5\Psi_n$ and of $^3\Psi_{ct}/^7\Psi_{ct}$) independent of the level of theory. The relative energies of the regular and charge-transfer states, however, depend strongly on the level of theory. At the HF and MP2 levels the charge-transfer states are several hundreds of kilojoules per mole higher in energy than the regular states, while the B3LYP method predicts that the charge-transfer states are lowest in energy by approximately 90 kJ mol^{-1}. The HF and MP2 methods rely on a single-reference wave function for describing the system, which can be problematic when several open-shell orbitals are present, and MCSCF calculations are required to probe the multiconfigurational nature of the above states. The active space for the MCSCF wave functions is of the orbital-restricted type,[25] where a full configurational space for the five d orbitals on Fe is combined with a full configurational space for the seven f orbitals on Nd. For the regular states the two spaces have five and three electrons, respectively, whereas the charge-transfer states have four electrons in each space. Dynamical electron correlation has been taken into account by second-order perturbation theory using the HF or MCSCF reference wave function.[26] The natural orbital occupancies from the MCSCF wave functions indicate that both the charge-transfer ($^7\Psi_{ct}$, $^5\Psi_{ct}$, $^3\Psi_{ct}$) and regular ($^5\Psi_n$, $^3\Psi_n$) states only contain a modest amount of multiconfigurational character.[27] The MCSCF and corresponding second-order perturbation methods give relative energies that are very similar to those at the single-reference HF and MP2 level, which suggests that the inclusion of multireference character in the wave function only has a minor influence on the results.

The double-zeta results in Table 3 have been extended by HF, MP2, and B3LYP calculations with a larger polarized triple-zeta-type basis set, in which only 28 and 10 core electrons in Nd and Fe, respectively, are modeled by an effective core potential, and these results are shown in Table 4. The small energy difference (few kJ mol^{-1}) between AF and FC couplings of the two spin centers is also found with the larger basis set. Compared with the results in Table 3, the use of the larger basis set preferentially stabilizes the

Table 3. Energy difference between different spin states [kJ mol^{-1}] as a function of the level of theory. The calculations employed the SBKJC effective core potential for Nd, Fe, C, N, and O,[32] and a polarized valence double-zeta basis set for the remaining electrons.[a]

Fe	Nd	State	Level	$<S^2>$	s_{Fe}	$s_{Fe(CN)_6}$	s_{Nd}	q_{Fe}	$q_{Fe(CN)_6}$	q_{Nd}	E_{rel}	E_{rel} (MP2)
↑↑↑↓↓	↑↑↑	$^5\Psi_n$	HF	6.06	1.3	1.0	3.0	−1.0	−2.8	2.3	0	0
			MCSCF					−1.3	−2.8	2.3	0	0
			B3LYP	6.29	1.4	1.3	3.0	−1.4	−2.4	1.6	0	
↑↑↓↓↓	↑↑↑	$^3\Psi_n$	HF	3.06	−1.3	−1.0	3.0	−1.0	−2.8	2.3	2	2
			MCSCF					−1.3	−2.8	2.3	0	0
			B3LYP[b]	3.08	−1.2	−1.0	3.1	−1.4	−2.5	1.6	3	
↑↑↑↓	↑↑↑↑	$^7\Psi_{ct}$	HF	12.67	3.4	2.0	4.0	−1.1	−1.9	1.6	362	221
			MCSCF					−1.5	−1.9	1.7	411	266
			B3LYP	12.06	2.1	2.0	4.0	−1.4	−1.8	1.2	−88	
↑↑↓↓	↑↑↑↑	$^5\Psi_{ct}$	HF	7.04	0.1	0.0	4.0	−1.1	−1.9	1.6	503	210
			MCSCF					−1.5	−1.9	1.7	411	206
			B3LYP[c]	6.82	0.3	0.2	3.8	−1.4	−1.9	1.2	−40	
↑↓↓↓	↑↑↑↑	$^3\Psi_{ct}$	HF	4.68	−3.4	−2.0	4.0	−1.1	−1.9	1.6	361	225
			MCSCF					−1.5	−1.9	1.7	411	265
			B3LYP	4.02	−2.1	−1.9	4.0	−1.4	−1.9	1.2	−89	

[a] Ψ_n denotes $Fe(d^5)/Nd(f^3)$ configurations and Ψ_{ct} denotes $Fe(d^4)/Nd(f^4)$ configurations. MCSCF indicates an orbital-restricted MCSCF with two CASSCF spaces, one consisting of the five d_{Fe} orbitals and the other of the seven f_{Nd} orbitals. The last column contains results in which electron correlation is included by second-order perturbation theory. s_{Fe} denotes the net spin on Fe, $s_{Fe(CN)_6}$ denotes the net spin on the whole $Fe(CN)_6$ complex, and s_{Nd} denotes the net spin on Nd. All net spins are in number of electrons with positive and negative numbers indicating excess alpha and beta spin, respectively. q indicates Mulliken atomic charges. [b] Unstable solution, collapses to the $^3\Psi_{ct}$ state upon reoptimization. [c] Unstable solution, unable to reoptimize due to numerical problems.

Table 4. Energy difference between different spin states [kJ mol^{-1}] as a function of the level of theory. The calculations employed the Stuttgart effective core potential for Nd and Fe,[33] whereas the remaining electrons were described using a 2d1f-polarized valence triple-zeta basis set.[34] Symbols have the same meaning as in Table 3.

Fe	Nd	State	Level	$<S^2>$	s_{Fe}	$s_{Fe(CN)_6}$	s_{Nd}	q_{Fe}	$q_{Fe(CN)_6}$	q_{Nd}	E_{rel}	E_{rel} (MP2)
↑↑↑↓↓	↑↑↑	$^5\Psi_n$	HF	9.11	1.3	0.7	3.9	0.3	−2.6	2.0	150	295
↑↑↓↓↓	↑↑↑	$^3\Psi_n$	HF	6.08	−1.3	−1.3	3.9	0.3	−2.6	2.0	150	297
↑↑↑↓	↑↑↑↑	$^7\Psi_{ct}$	HF	14.67	3.5	1.9	4.4	0.1	−1.9	1.8	0	0
			B3LYP	14.09	2.2	1.8	4.7	−0.5	−1.9	1.6	0	
↑↑↓↓	↑↑↑↑	$^5\Psi_{ct}$	HF	9.06	0.2	−0.1	4.4	0.2	−1.9	1.8	137	−25
			B3LYP	9.04	0.0	−0.2	4.7	−0.5	−1.8	1.6	52	
↑↓↓↓	↑↑↑↑	$^3\Psi_{ct}$	HF	6.81	−3.5	−2.1	4.5	0.1	−1.9	1.8	−1	15
			B3LYP	6.08	−2.3	−2.2	4.7	−0.5	−1.8	1.6	−5	

charge-transfer states, such that they are now several hundreds of kilojoules per mole lower in energy at the HF and MP2 levels of theory. It was not possible to converge solutions corresponding to $^3\Psi_n$ or $^5\Psi_n$ states at the B3LYP level, most likely because these are substantially higher in energy than the charge-transfer states.

The results in Tables 3 and 4 indicate that there is only a weak coupling between the two spin centers in the complex, and it is unlikely that this will be changed by crystal effects. It is therefore difficult to reconcile the observed geometry changes upon excitation with a change from an AF to a FC coupling.[21] The calculations, however, suggest that the excitation may correspond to a charge-transfer process in which the Fe(d^5)/Nd(f^3) configuration is changed to an Fe(d^4)/Nd(f^4) configuration. The former will most likely be a Boltzmann mixture of triplet and pentet states, whereas the latter will be a Boltzmann mixture of triplet and septet states, and perhaps also pentet states, which thereby accounts for the increase in magnetic moment. With the present computational approaches it is not possible to establish a reliable energy ordering of these two types of configuration, as the results depend significantly on both the wave function and the basis set. It is furthermore likely that crystal effects will also contribute to the relative stability, but the calculations suggest that both types of configurations are energetically possible. Thus, it is postulated that the excitation process involves charge transfer from the {Fe(CN)$_6$} moiety to {Nd(dmf)$_4$(H$_2$O)$_3$}, which leads to a geometry change in which the charge-transfer state is metastable.

Analysis of the wave functions in terms of Mulliken atomic charges (Tables 3 and 4) suggests that there is only a very small change in the electron density around the Fe atom between the $^{3/5}\Psi_n$ and $^{3/5/7}\Psi_{ct}$ states, and the latter may even have a slightly larger electron density around Fe despite the formal transfer of charge from {Fe(CN)$_6$} to {Nd(dmf)$_4$(H$_2$O)$_3$}. This is in agreement with the Mössbauer data reported by Li et al., [17] which showed that the Fe valence state is unchanged upon UV illumination of the crystal. The calculated charges suggest that the primary charge transfer is from the cyanide ligands on {Fe(CN)$_6$} to the {Nd(dmf)$_4$(H$_2$O)$_3$} complex, where most of the transferred charge resides on the Nd atom.

To directly probe the nature of the excitation process, time-dependent HF calculations have been performed using the $^3\Psi_n$ and $^5\Psi_n$ states as reference wave functions. These calculations indicate that there are a large number of low-lying excited states, but most of these have vanishing transition probabilities. The lowest excited states with appreciable transition strength ($f \approx 0.02$) have calculated excitation wavelengths in the range 300–345 nm, which is at a slightly shorter wavelength than in the experiments, but time-dependent HF calculations are known to overestimate excitation energies. A density difference plot for the excited states with appreciable transition strengths indicates that several of the excitations involve transfer of charge from the cyanide ligands to the Nd atom and/or dmf ligands. These results are thus consistent with a mechanism in which short wavelength light induces a charge transfer from the cyanide ligands to the Nd atom, followed by a reorganization of the spin state on the {Fe(CN)$_6$} complex, and a change in geometry that produces a metastable charge-transfer state.

The photomagnetic effect: The theoretical evidence for a charge-transfer mechanism from {Fe(CN)$_6$} to Nd in the metastable state is in agreement with the observed structural changes in **1**. The charge transfer is mainly taking place from the cyano ligands in agreement with the increased cyano bond lengths and shorter Fe–C bond lengths. Whereas **1**, **3**, and **4** show a very similar structural response to UV illumination, and **5** shows similar cell changes, apparently **2** does not undergo any structural modification. On the other hand, **2** is photomagnetic when irradiated with visible light.[19] It appears that the same mechanism must be involved in the excitation process in all the iron-containing complexes. Thus, the iron atom and the cyano ligands must play an essential role in the excitation, in which the choice of the lanthanide ion is secondary. It is not known, however, whether **3**, **4**, and **5** show changes in their magnetization properties in the metastable state, and this is the subject of an ongoing investigation. According to Akitsu et al., only Nd-containing complexes with the general formula [Ln(dmf)$_4$(H$_2$O)$_3$M(CN)$_6$]·H$_2$O exhibit photoinduced magnetic phenomena,[28] but this conclusion was based on studies of one single compound, [Gd(dmf)$_4$(H$_2$O)$_3$Cr(CN)$_6$]·H$_2$O.[29] Since the present data reveal similar structural changes upon UV illumination for **1**, **3**, and **4**, and since **5** also appears to be photoactive, it seems plausible that other complexes can exhibit photomagnetic behavior.

Even though the theoretical calculations focus on **1**, we anticipate that the isostructural complexes have similar charge transferabilities in the same energy range, since the lanthanide atom is not expected to have much influence on the molecular orbitals around the iron atom. This indicates that **3**, **4**, and **5** will show changes in their magnetic moment upon excitation due to more unpaired spin in the cyano ligands and on the lanthanide atom. This hypothesis does not contradict the Mössbauer results by Li et al. even though a charge-transfer mechanism between the two metal ions was ruled out earlier. The theoretical analysis indicates that charge is moved from the cyano ligands to the other metal center, and to a first approximation the charge density around the Fe atom is therefore not affected.

Even though an excitation of **2** was not possible by UV-light irradiation, it does not contradict the earlier observation of its photoinduced behavior upon visible-light illumination.[14] A test experiment on **1** was performed using visible light with a wavelength of 532 nm but as expected no cell changes were observed. For **1** only UV light causes a photoexcitation. The only difference between **1** and **2** is the substitution of Fe with Co, and hence we expect the same mechanism to be active, although shifted in energy due to the different nature of Fe and Co.

Conclusion

Single-crystal X-ray diffraction combined with UV-laser illumination has revealed the ground- and excited-state structures of the photomagnetic heterobimetallic complexes **1**, **3**, and **4**. Similar structural changes were observed upon illumination, with the largest modifications observed in the iron–ligand bond lengths and in the C–N bond length. Photoactive behavior was also observed for **5** (unit-cell changes), but it was not possible to determine the excited-state structure of this complex. The observations indicate that the iron atom plays an important role in the UV excitation process. Theoretical analysis of **1** suggests that charge transfer from the cyano ligands to the lanthanide atoms can explain the photomagnetic effect in good agreement with the observed structural changes. Apparently the importance of the lanthanide atoms is secondary to the transition metal (Fe vs. Co), since all the iron complexes show the same pattern of bond-length changes. This suggests that the same mechanism is responsible for the excitation for all the iron complexes, and these complexes are therefore expected to show a similar photomagnetic behavior to that observed for **1**.

Experimental Section

Synthesis: The five different compounds (**1**–**5**) were synthesized by mixing $K_3[Fe(CN)_6]$ (or $K_3[Co(CN)_6]$) (1 mmol) with water (10 mL). A lanthanide salt (1 mmol) dissolved in DMF (5 mL) was then added down the side of the glass very slowly. $NdCl_3$ was used for the Nd compound and $[Ln(NO_3)_3]$ was used for Ln = Gd, Y, and La, respectively. Green-yellow crystals precipitated and crystals suitable for single-crystal X-ray analysis were obtained after evaporation. All the compounds **1**, **2**, **3**, and **4** are isostructural and crystallize in the $P2_1/n$ space group. The **5** system crystallizes in the $P2_1/c$ space group, but the crystal structure has an identical molecular conformation as well as highly similar intermolecular contacts. All crystals have four asymmetric ($[Ln(C_3H_7NO)_4Fe(CN)_6]\cdot H_2O$) units per unit cell. The molecules are connected to each other through hydrogen bonds formed with the crystal water molecule (see Figure 1 of ref. [21]).

Photocrystallography: Single-crystal X-ray diffraction experiments with and without UV illumination were carried out at University of Rennes 1, France, using $Mo_{K\alpha}$ radiation on an Oxford Diffraction Xcalibur3 diffractometer equipped with a CCD detector. The dimensions of the crystals were approximately 150–200 μm. They were attached with oil on a goniometer head before being mounted on the diffractometer. Data were collected at 15 K using a HeliJet cryocooler. The light source was an UV diode with an emission wavelength of (390 ± 10) nm. The diode was held fixed during the entire experiments, and the light was focused on the crystals by a lens. The excitation density at the crystals was around 100 mW cm^{-2}. For each crystal a ground-state data collection consisting of four different ω scans and lasting approximately 3 h was made (data collection #0) before turning on the UV diode. After turning on the laser diode, the exact same data collection was repeated 3 to 7 times depending on the capacity of the liquid helium tank. Each 3 h data set was analyzed independently to follow structural changes as a function of time. The data collection and reduction were performed with the programs CrysAlis CCD and CrysAlis RED.[30] No absorption correction was performed. The structures were refined with SHELXL-97.[31] All non-water hydrogen atoms were refined as riding on the parent C atom. The ground-state data collection (#0) was refined using a single conformer with full occupancy on all sites. All atoms except hydrogen were treated anisotropically. The ground-state fractional coordinates were then imported into the refinement of the last data collection, where two conformers were co-refined: an excited-state structure and a fixed ground-state structure. The sum of their occupancies was constrained to unity. Restraints were imposed on the bond lengths in the dmf ligands of the excited state. For **1** and **4** the atoms in the dmf groups 20 and 40 together with all hydrogen atoms were modeled isotropically, while all other atoms in the excited-state conformer were refined with anisotropic atomic displacement parameters (ADPs). For **3**, all nonmetallic atoms were refined with isotropic ADPs. The structural models of the excited states (fractional coordinates and ADPs) obtained from the last data collections and the ground-state models were then imported and kept fixed in the refinements of the remaining data collections, where only the scale factor and the occupancy were refined. An analysis of the data using only one conformer has also been performed, thereby obtaining an average structure of the ground-state and the excited-state structure. These average models showed the exact same bond-length tendencies as the excited-state structures obtained from the two conformer models, though not as evident.

To investigate the reversibility of the photomagnetic effect, crystal **1** was taken out of the cold stream and UV light after measuring the last data collection. According to Li et al., the photomagnetic behavior should vanish at temperatures above 50 K. Unfortunately, the crystal did not survive this sudden change in temperature, and it was therefore not possible to examine whether the crystal had returned to the ground state. CCDC-745262, 745263, 745264, 745265, 745266, and 745267 (**4**); 745268, 745269, 745270, and 745271 (**3**); and 745272 (**5**) contain the supplementary crystallographic data for this paper. These data can be obtained free of charge from The Cambridge Crystallographic Data Centre via www.ccdc.cam.ac.uk/data_request/cif.

Theoretical calculations: Theoretical calculations have been performed on complex **1** using the experimental ground-state geometry from the photocrystallographic experiment. A first series of calculations employed the SBKJC effective core potential for Nd, Fe, C, N, and O, which replace 46, 10, 2, 2, and 2 core electrons, respectively, by a model potential.[32] The remaining valence electrons were described by a polarized va-

lence double-zeta basis set. Another series of calculations employed the Stuttgart effective core potential for Nd and Fe, which replace 28 and 10 core electrons, respectively, with an effective core potential.[33] The remaining electrons were described using a 2d1f-polarized valence triple-zeta basis set.[34] Decomposition of the wave function spin and charge into atomic contributions was done by using the Mulliken procedure. Single-reference calculations have been performed using the Gaussian 03 program package,[35] and the GAMESS-US program package has been used for the multireference calculations.[36]

Acknowledgements

This work was supported by grants from the Danish Center for Scientific Computation, the Danish Natural Science Research Council, and the Danish National Research Foundation.

[1] a) P. Coppens, I. Novozhilova, A. Kovalevsky, *Chem. Rev.* **2002**, *102*, 861–883; b) P. Coppens, *Chem. Commun.* **2003**, 1317–1320; c) J. M. Cole, *Acta Crystallogr. Sect. A* **2008**, *64*, 259–271; d) K. Ichiyanagi, J. Herbert, L. Toupet, H. Cailleau, P. Guionneau, J.-F. Létard, E. Collet, *Phys. Rev. B* **2006**, *73*, 060408; e) V. Legrand, S. Pillet, C. Carbonea, M. Souhassou, J.-F. Létard, P. Guionneau, C. Lecomte, *Eur. J. Inorg. Chem.* **2007**, 5693–5706; f) J. M. Cole, *Z. Kristallogr.* **2008**, *223*, 363–369.

[2] J. M. Cole, *Chem. Soc. Rev.* **2004**, *33*, 501–513.

[3] M. Rüdlinger, J. Schefer, T. Vogt, T. Woike, S. Haussühl, H. Zöllner, *Physica B+C* **1992**, *180*, 293–298.

[4] M. D. Carducci, M. R. Pressprich, P. Coppens, *J. Am. Chem. Soc.* **1997**, *119*, 2669–2678.

[5] a) A. Y. Kovalevsky, K. A. Bagley, P. Coppens, *J. Am. Chem. Soc.* **2002**, *124*, 9241–9248; b) A. Y. Kovalevsky, K. A. Bagley, J. M. Cole, P. Coppens, *Inorg. Chem.* **2003**, *42*, 140–147.

[6] K. F. Bowes, J. M. Cole, S. L. G. Husheer, P. R. Raithby, T. L. Savarese, H. A. Sparkes, S. J. Teat, J. E. Warren, *Chem. Commun.* **2006**, 2448–2450.

[7] J. Kusz, H. Spiering, P. Gütlich, *J. Appl. Crystallogr.* **2001**, *34*, 229–238.

[8] N. Huby, L. Guérin, E. Collet, L. Toupet, J. C. Ameline, H. Cailleau, T. Roisnel, T. Tayagaki, K. Tanaka, *Phys. Rev. B* **2004**, *69*, 020101(R).

[9] S. Pillet, V. Legrand, H. P. Weber, M. Souhassou, J. F. Létard, P. Guionneau, C. Lecomte, *Z. Kristallogr.* **2008**, *223*, 235–249.

[10] E. Trzop, M. B. L. Cointe, H. Cailleau, L. Toupet, G. Molnar, A. Bousseksou, A. B. Gaspar, J. A. Real, E. Collet, *J. Appl. Crystallogr.* **2007**, *40*, 158–164.

[11] a) C. D. Kim, S. Pillet, G. Wu, W. K. Fullagar, P. Coppens, *Acta Crystallogr. Sect. A* **2002**, *58*, 133–137; b) Y. Ozawa, M. Terashima, M. Mitsumi, K. Toriumi, N. Yasuda, H. Uekusa, Y. Ohashi, *Chem. Lett.* **2003**, *32*, 62–63; c) N. Yasuda, M. Kanazawa, H. Uekusa, Y. Ohashi, *Chem. Lett.* **2002**, 1132–1133.

[12] E. Collet, M. H. Lemée-Cailleau, M. B. L. Cointe, H. Cailleau, M. Wulff, T. Luty, S. Y. Koshihara, M. Meyer, L. Toupet, P. Rabiller, S. Techert, *Science* **2003**, *300*, 612–615.

[13] O. Sato, *J. Photochem. Photobiol. C* **2004**, *5*, 203–223.

[14] Y. Einaga, *J. Photochem. Photobiol. C* **2006**, *7*, 69–88.

[15] O. Sato, T. Iyoda, A. Fujishima, K. Hashimato, *Science* **1996**, *272*, 704–705.

[16] T. Korzeniak, C. Mathenière, A. Kaiba, P. Guionneau, M. Koziel, *Inorg. Chim. Acta* **2008**, *361*, 3500–3504.

[17] G. Li, T. Akitsu, O. Sato, Y. Einaga, *J. Am. Chem. Soc.* **2003**, *125*, 12396–12397.

[18] a) J. Overgaard, H. Svendsen, M. A. Chevallier, B. B. Iversen, *Acta Crystallogr. Sect. E* **2005**, *61*, m268–m270; b) H. Svendsen, J. Overgaard, M. A. Chevalier, B. B. Iversen, *Acta Crystallogr. Sect. E* **2006**, *62*, m989–m991; c) S. Tanase, J. Reedijk, *Coord. Chem. Rev.* **2006**, *250*, 2501–2510.

[19] G. Li, O. Sato, T. Akitsu, Y. Einaga, *J. Solid State Chem.* **2004**, *177*, 3835–3838.

[20] G. Li, P. Yan, O. Sato, Y. Einaga, *J. Solid State Chem.* **2005**, *178*, 36–40.

[21] H. Svendsen, J. Overgaard, M. A. Chevalier, E. Collet, B. B. Iversen, *Angew. Chem.* **2009**, *121*, 2818–2821; *Angew. Chem. Int. Ed.* **2009**, *48*, 2780–2783.

[22] A. Figuerola, C. Diaz, J. Ribas, V. Tangoulis, J. Granell, F. Lloret, J. Mahía, M. Maestro, *Inorg. Chem.* **2003**, *42*, 641–649.

[23] For example, see: a) R. Haser, C. E. De Broin, M. Pierrot, *Acta Crystallogr. Sect. B* **1972**, *28*, 2530–2537; b) P. M. Pierrot, R. Kern, R. Weiss, *Acta Crystallogr.* **1966**, *20*, 425–428.

[24] M. R. Warren, S. K. Brayshaw, A. L. Johnson, S. Schiffers, P. R. Raithby, T. L. Easun, M. W. George, J. E. Warren, S. J. Teat, *Angew. Chem.* **2009**, *121*, 5821–5824; *Angew. Chem. Int. Ed.* **2009**, *48*, 5711–5714.

[25] J. Ivanic, *J. Chem. Phys.* **2003**, *119*, 9364–9376; J. Ivanic, *J. Chem. Phys.* **2003**, *119*, 9377–9385.

[26] H. Nakano, *J. Chem. Phys.* **1993**, *99*, 7983–7992.

[27] For the charge transfer states, the natural orbital occupancy numbers are (1.93, 1.00, 0.99, 0.07, 0.01) and (1.00, 1.00, 1.00, 1.00, 0.00, 0.00, 0.00) for the two orbital spaces, respectively, while the corresponding values for the regular states are (1.97, 1.96, 1.00, 0.04, 0.03) and (1.00, 1.00, 1.00, 0.00, 0.00, 0.00, 0.00).

[28] T. Akitsu, Y. Einaga, *Chem. Pap.* **2007**, *61*, 194–198.

[29] T. Akitsu, J. Nishijo, *J. Magn. Magn. Mater.* **2008**, *320*, 1586–1590.

[30] Oxford Diffraction, CrysAlis CCD and CrysAlis RED., Oxford Diffraction Ltd, Abingdon, Oxfordshire, **2007**.

[31] SHELX-97—Programs for Crystal Structure Analysis, Release 97–92, G. M. Sheldrick, University of Göttingen, Göttingen, **1998**.

[32] a) J. S. Binkley, J. A. Pople, W. J. Hehre, *J. Am. Chem. Soc.* **1980**, *102*, 939; b) W. J. Stevens, H. Basch, M. Krauss, *J. Chem. Phys.* **1984**, *81*, 6026; c) W. J. Stevens, M. Krauss, H. Basch, P. G. Jasien, *Can. J. Chem.* **1992**, *70*, 612; d) T. R. Cundari, W. J. Stevens, *J. Chem. Phys.* **1993**, *98*, 5555.

[33] D. Andrae, U. Haeussermann, M. Dolg, H. Stoll, H. Preuss, *Theor. Chim. Acta* **1990**, *77*, 123–141.

[34] F. Weigend, R. Ahlrichs, *Phys. Chem. Chem. Phys.* **2005**, *7*, 3297–3305.

[35] Gaussian 03, Revision C.02, M. J. Frisch, G. W. Trucks, H. B. Schlegel, G. E. Scuseria, M. A. Robb, J. R. Cheeseman, J. A. Montgomery, Jr., T. Vreven, K. N. Kudin, J. C. Burant, J. M. Millam, S. S. Iyengar, J. Tomasi, V. Barone, B. Mennucci, M. Cossi, G. Scalmani, N. Rega, G. A. Petersson, H. Nakatsuji, M. Hada, M. Ehara, K. Toyota, R. Fukuda, J. Hasegawa, M. Ishida, T. Nakajima, Y. Honda, O. Kitao, H. Nakai, M. Klene, X. Li, J. E. Knox, H. P. Hratchian, J. B. Cross, V. Bakken, C. Adamo, J. Jaramillo, R. Gomperts, R. E. Stratmann, O. Yazyev, A. J. Austin, R. Cammi, C. Pomelli, J. W. Ochterski, P. Y. Ayala, K. Morokuma, G. A. Voth, P. Salvador, J. J. Dannenberg, V. G. Zakrzewski, S. Dapprich, A. D. Daniels, M. C. Strain, O. Farkas, D. K. Malick, A. D. Rabuck, K. Raghavachari, J. B. Foresman, J. V. Ortiz, Q. Cui, A. G. Baboul, S. Clifford, J. Cioslowski, B. B. Stefanov, G. Liu, A. Liashenko, P. Piskorz, I. Komaromi, R. L. Martin, D. J. Fox, T. Keith, M. A. Al-Laham, C. Y. Peng, A. Nanayakkara, M. Challacombe, P. M. W. Gill, B. Johnson, W. Chen, M. W. Wong, C. Gonzalez, and J. A. Pople, Inc., Wallingford CT, **2004**.

[36] M. W. Schmidt, K. K. Baldridge, J. A. Boatz, S. T. Elbert, M. S. Gordon, J. H. Jensen, S. Kosecki, N. Matsunaga, K. A. Nguyen, S. J. Su, T. L. Windus, M. Dupuis, J. A. Montgomery, *J. Comput. Chem.* **1993**, *14*, 1347–1363.

Received: October 29, 2009
Published online: May 12, 2010

